Establishing the Role of Graphite as a Shaping Agent of Vanadium–Aluminum Mixed (Hydr)oxides and Their Physicochemical Properties and Catalytic Functionalities

Víctor G. Baldovino-Medrano,* Benjamin Farin, and Eric M. Gaigneaux*

Institute of Condensed Matter and Nanosciences-IMCN, Division Molecules, Solids and Reactivity, Université Catholique de Louvain, Croix du Sud 2/17, B-1348 Louvain-la-Neuve, Belgium

Ⓢ *Supporting Information*

ABSTRACT: This work contributes to the establishment of a scientific basis for the understanding of the effect of shaping on the physicochemical properties and functionalities of catalytic powders. In particular, the influence of graphite (G) as a shaping agent for vanadium–aluminum mixed (hydr)oxides, VAlO, is presented herein. Graphite was added in different loadings (x = 1, 3, and 7 wt %). VAlO-xG hydroxides were tableted and then calcined as to obtain VAlO-xG mixed oxides. Both series of materials were characterized and tested in propane oxidative dehydrogenation (ODH). Correlation of X-ray photoelectron spectrometry (XPS) and Raman data permitted establishing that VAlO-xG hydroxides are constituted by graphite particles physically attached to the amorphous VAlO structure. The VAlO hydroxide structure was found to be composed of $Al(OH)_3$ and AlOOH linked to decavanadates-, metavanadates, and isolated or cluster vanadyl V=O species. Calcination of VAlO-xG caused further polymerization of vanadium species into decavanate chains and V_2O_5-like structures connected to a γ-Al_2O_3-like matrix. Though graphite was not incorporated into the structure of VAlO, XPS analysis showed that it actively interacts with the VAlO surface. Such interaction favored propylene selectivity in ODH. Particularly, graphite containing VAlO-xG displayed higher production of propene over CO_x at high propane conversion. On the other hand, though graphite boosts the mechanical resistance of the VAlO-xG tablets, the surface area of the materials, as determined by the application of χ-theory, was found to significantly decrease after shaping and further calcination. This trend was explained considering pore widening during tableting. Finally, characterization performed on particles recovered from crushed VAlO-xG tablets showed that graphite particles were randomly distributed within the shaped catalysts.

KEYWORDS: *VAlO mixed (hydr)oxides, graphite, shaping, N_2 physisorption, XPS, Raman, propane ODH*
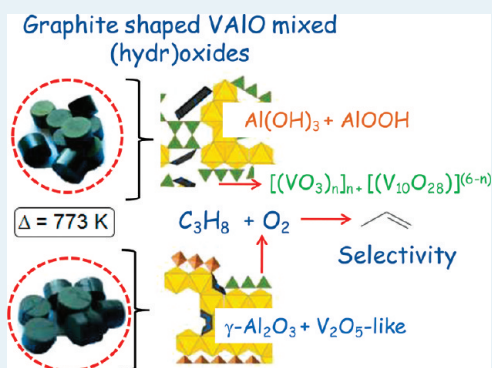
1. INTRODUCTION

When a catalyst is going to be implemented at the industrial scale, shaping of the synthesized powder is an essential step.[1] The utilization of shaped catalytic bodies instead of irregular and small particles (250 μm ≤ Dp ≤ 500 μm) in an industrial reactor is compulsory because the latter cause excessive pressure drops and thereafter reactor plugging, premature catalyst replacement, and eventual plant shut down.[1] The shape of the catalyst body itself is to be considered to achieve uniform flow and heat transfer patterns inside the reactor.[2] Shaping is normally performed by extrusion or tableting of the catalytic powder with the aid of binders, lubricants and other additives.[3] Inorganic binders become a permanent component of the formed catalyst. Even though it is aimed that such substances not change the catalytic performance of the materials, they can completely or partially modify their functionalities.[1–4] As an example, Font Freide et al.[4] reported on the difficulties encountered when trying to find a suitable binding agent for a catalyst aimed to be employed in an industrial Fischer–Tropsch process. Another report[5] showed that for faujasite

zeolite the interaction between silica from the binder and active alumina from the zeolite led to the formation of Lewis acid sites under a Fluid Catalytic Cracking reaction environment which deeply impact the catalyst's lifespan. Busca[2] highlighted how silica and alumina oxides binders besides changing the mechanical and textural properties (porosity) of zeolites can serve to tune their catalytic functionalities to certain specific requirements. Nevertheless, as shaping is only considered during the scaling-up of catalytic materials it rather remains an art protected under industrial secrecy,[6,7] thus often escaping thorough scientific scrutiny. It has only been in recent years that in-depth studies aiming to understand the influence of shaping on the physicochemical properties and functionalities of catalytic materials at a more fundamental level have begun to be published.[8–12] These studies have commenced to change the paradigm that binding agents must be inert substances only

intended to transform catalytic powders into mechanically resistant bodies.

The objective of this work is to contribute to the construction of a scientific basis for the comprehension of the molecular level modifications induced by binding agents for catalyst shaping. Particularly, herein we continue to investigate the role of graphite as a shaping agent of catalytic powders for selective oxidation reactions. A former study[12] conducted on bismuth molybdate (BiMo) catalysts for propylene partial oxidation to acrolein demonstrated that graphite improves the mechanical resistance of BiMo tablets. This time it was decided to study the effect of graphite as a shaping agent of vanadium−aluminum mixed (hydr)oxides (VAlOs). These materials are precursors of vanadium−aluminum oxynitrides (VAlONs) catalysts employed in ammoxidation reactions.[13−16] The chosen model reaction was the oxidative dehydrogenation (ODH) of propane to propylene which remains of academic, practical, and environmental interest.[1,17,18] The research methodology consisted on characterizing VAlOs at different stages of the preparation process and shaping as well as before and after the catalytic tests.

2. EXPERIMENTAL METHODS

2.1. Catalysts Preparation. Vanadium−aluminum mixed (hydr)oxides were prepared at the 1 kg scale using the coprecipitation technique and the experimental setup described by Prada Silvy et al.[13] Ammonium metavanadate (NH_4VO_3, Isochim, technical degree) and aluminum nitrate nonahydrate ($Al(NO_3)_3 \cdot 9H_2O$, Merck, 95%) were used as vanadium and aluminum precursors, respectively. The amount of both precursors was fixed so as to obtain a V/Al ratio = 0.25 in the VAlO material. First, NH_4VO_3 was dissolved at $T = 333$ K in the required volume of water so as to obtain a vanadium concentration of 0.030 M in the solution. The pH of the solution was adjusted to 3 by the addition of HNO_3 (Merck, 65%). Next, $Al(NO_3)_3 \cdot 9H_2O$ was added and then the pH of the solution was increased to 5.5 by the addition of NH_4OH (Merck, 25%). Coprecipitation was allowed to proceed under these conditions for 30 min under constant stirring with a boat propeller type stirrer. The obtained yellow VAlO mixed hydroxide was filtered in a belt-filter and then washed overnight under stirring with hot water in the coprecipitation reactor vessel. After a second filtration, the recovered solid was dried in a static air stove at 333 K.

The dried VAlO hydroxide powder was tableted in a hand-operated machine (Ateliers Ed. Courtoy, series 796). Cylindrical tablets of 2.3 mm length and 5.1 mm of diameter were obtained by fixing the separation between the two pistons that compress the powder. Graphite (G) (Merck, technical grade) was used as a binding agent, and the effect of its loading was studied by varying its nominal content from 0, 1, 3, to 7 wt %. The VAlO hydroxide was ground and sieved to a particle size lower than 100 μm before mixing it with graphite in a glass container. Mixing of these two powders was performed by rolling over the glass container during about 15 min. The VAlO-graphite tablets were named VAlO-xG after its graphite content; x being the nominal graphite content.

Some of the produced VAlO-xG tablets were calcined in a static air oven at 773 K for 4 h to convert the hydroxides into mixed oxides. To differentiate the calcined catalysts from the noncalcined ones the indexes C, calcined, and NC, noncalcined, were added to their respective nomenclature. For example, VAlO-3G-NC stands for a noncalcined VAlO catalyst

containing 3 wt % graphite and VAlO-3G-C for the corresponding calcined one. Finally, the index −NT = nontableted was added to those catalysts which were not submitted to tableting. Nontableted VAlO-NC-NT and VAlO-NC-T were characterized and used as references in the analysis of the tableted materials.

2.2. Materials Characterization. *2.2.1. N_2 Physisorption Experiments.* N_2 adsorption−desorption isotherms at 77 K were measured by the volumetric method in a Micromeritics Tristar 3000 apparatus. The analysis was performed on pure graphite and VAlO-xG-NC/C particles of size range 100−350 μm recovered after crushing the corresponding tablets. In general, 0.15−0.25 g of sample were outgassed overnight at 423 K under a vacuum pressure of 15 Pa before running the analyses. Under these conditions, the samples of noncalcined VAlO-xG-NC lost an average weight of 20% while calcined VAlO-xG-C catalysts lost about 10 wt % of their weight after the outgassing step. During each test, both the warm and the cold free spaces of the sample cells were automatically measured by the apparatus. The relative pressure (P/P_0) range of the measurements was comprised between 0.01−0.99 with 59 points being collected to complete the isotherms. The surface area of samples of nontableted VAlO before (VAlO-NC-NT) and after calcination (VAlO-C-NT) were taken as references in regard to the other samples. The reproducibility of the measurements, as determined from the analysis of three samples of VAlO-NC-NT in different runs, was determined to be about 10%.

2.2.2. Scanning Electron Microscopy (SEM). SEM micrographs of VAlO-xG particles recovered after crushing tablets were taken with a JSM-35C, JEOL scanning electron microscope.

2.2.3. Mechanical Resistance. The compressive strength (σ_ε) of the VAlO-xG-NC/C tablets was measured in an automatic Instron 5566 machine using the same methods reported elsewhere.[12] The compressive strength was determined from the average of the values read in five measurements. The error in the calculated values was estimated as their standard deviation. The accuracy and reproducibility of the force measured during these tests were within the range ±1 N.

2.2.4. X-ray Photoelectron Spectrometry (XPS). XPS measurements were performed on a SSI-X-probe (SSX-100/ 206) photoelectron spectrometer (Surface Science Instruments) equipped with a monochromatic microfocused Al Kα X-ray source (1486.6 eV). For this analysis, fresh tablets were first ground in an agate mortar, and the obtained powder was then pressed into small stainless steel troughs mounted on a multispecimen ceramic holder. The pressure in the analysis chamber was around 1.3×10^{-6} Pa. The analyzed area was approximately 1.4 mm^2 (1000 μm × 1700 μm) and the pass energy was 150 eV. Under these conditions, the full width at half-maximum (fwhm) of the Au 4f$_{7/2}$ peak of a clean gold standard sample was about 1.6 eV. A flood gun set to 8 eV and a Ni grid placed 3 mm above the sample surface were used for charge stabilization. The following spectra were recorded: general spectrum, C 1s, O 1s + V 2p$_{3/2}$, Al 2p, N 1s, and C 1s again to check the stability of charge compensation as a function of time. The spectra were decomposed with the CasaXPS program (Casa Software Ltd., U.K.) with a Gaussian/ Lorentzian (85/15) product function after subtraction of a Shirley baseline. Further details on the analysis conditions were given in ref 19.
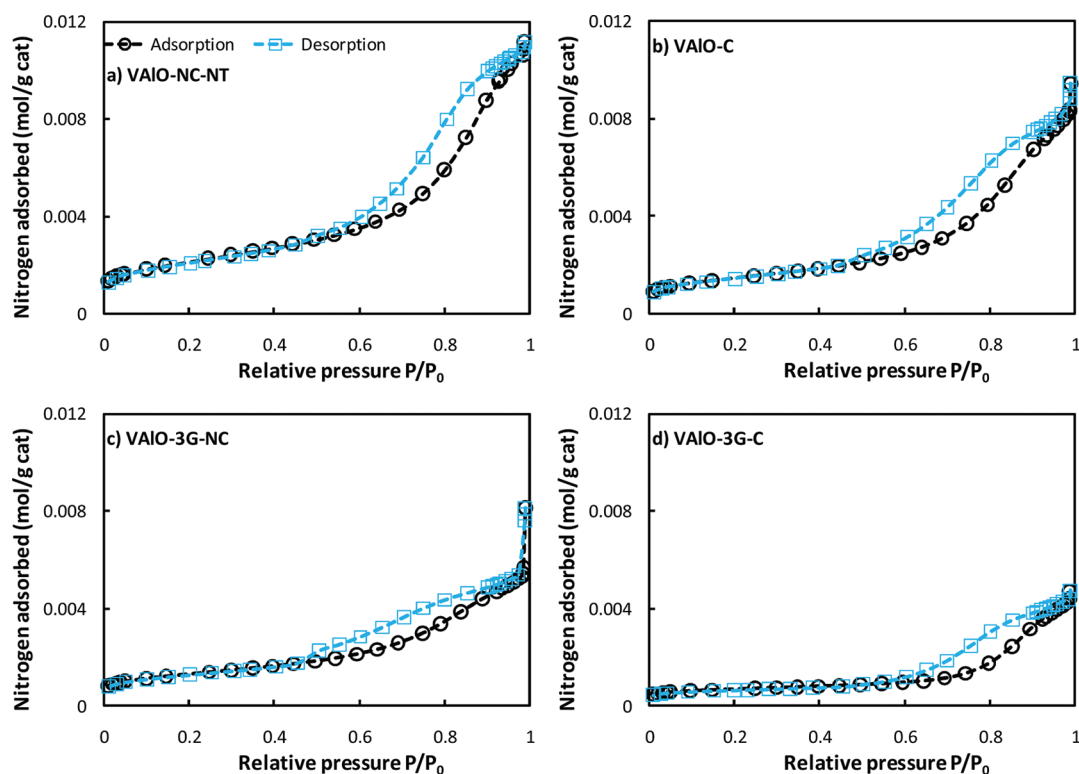
Figure 1. Nitrogen adsorption−desorption isotherms at 77 K of selected catalysts: (a) VAlO-NC-NT; (b) VAlO-C; (c) VAlO-3G-NC; and (d) VAlO-3G-C.

2.2.5. Raman Spectroscopy. Raman spectroscopy, as to determine the molecular structural arrangement of VAlO-xG, was perfomed with a confocal Thermo Scientific DXR Raman Microscopy system using an excitation laser source with a wavelength of 633 nm operating at a power of 6.5 mW. The 100× objective of the microscope was used to spot 50 μm of the surface of the sample to perform the analysis. Spectra were obtained by averaging 20 scans of the Raman shift range between 1900 and 100 cm^{-1} recorded in 20 s with a spectral resolution of 1 cm^{-1}. The identity of the spectra obtained at different positions of each sample was systematically verified.

2.3. Catalytic Tests. VAlO-xG materials were tested in the propane ODH to propylene reaction at 723 and 748 K using about 0.1 g of catalyst. Catalyst particles (500 < Dp ≤ 350 μm) recovered from crushed tablets were employed during the tests. These particles were mixed with 0.4 g of quartz spheres (Dp ≤ 200 μm) to warrant plug flow and put inside a U-shaped fixed bed quartz reactor. The dimensions of the reactor were as follows: external diameter of the tube = 0.6 cm; external diameter of the fixed bed = 1.4 cm; and length = 19.1 cm. The empty space between the entrance and exit of the fixed bed was not filled up. The reactor was provided with a thermowell located at the same height of the catalytic bed. This allowed a direct sensing and control of the reactor temperature at the level of the catalytic bed. Temperature was sensed by a K-type thermocouple connected to a conventional PID controller. A total gas feed flow of 40 mL/min with the composition C_3H_8/O_2/N_2 = 10/15/75 (vol %) was used. Technical grade propane, 99.999% purity oxygen, and 99.999% nitrogen were provided by Praxair and used as received. Reaction products identification was made online with a Varian GC provided with three columns and three detectors. A Hayesep column coupled with a Molecular Sieve column and a TCD detector

were used to separate and quantify O_2, N_2, CO, CO_2, C_3H_8, and C_3H_6. The presence and quantification of oxygenates was managed through a system composed by one EC-Wax column coupled with an FID detector. Traces of other oxygenated products were detected, but they were not quantified. Under such conditions, the carbon balance registered an error between 10−15%. The catalytic performance was calculated in terms of molar conversion of propane ($\%C_{C3H8}$) and oxygen ($\%C_{O2}$) and yield percentage to different reaction products: $\%y_{COx} = (\%y_{CO2} + \%y_{CO})$ and $\%y_{C3H6}$. Given the bulk nature of the catalyst, conversion and yields were further expressed as a function of catalyst weight ($gcat.$) and surface area; the latter as determined from N_2 physisorption experiments, hence:

$$a_i = \frac{\%C_i}{gcat. \times A_S} \tag{1}$$

where i = C_3H_8 or O_2; a_i = intrinsic activity [m^{-2}]; A_S = catalyst surface area in m^2/g.

$$y^i_j = \frac{\%y_j}{gcat. *A_S} \tag{2}$$

where j = C_3H_6 or CO_x; y^i = intrinsic yield [m^{-2}].

Consequently, selectivity to propene was defined as:

$$S_{C_3H_6} = \frac{\%y^i_{C_3H_6}}{\%y^i_{C_3H_6} + \%y^i_{CO_x}} \tag{3}$$

The absence of mass and heat transfer limitations was theoretically verified by calculating the Damköhler number[20] and the Weisz−Prater criterion[20,21] (for details please refer to the Supporting Information).

3. RESULTS AND DISCUSSION

3.1. Textural Properties of VAlO-xG-NC/C Catalysts.

In this section, the textural properties of the VAlO-xG-NC/C and graphite as determined from nitrogen adsorption−desorption at 77 K are presented and discussed. The shapes of the N_2 adsorption−desorption isotherms of the catalysts are discussed first before proceeding to the determination of the surface area. Surface area was initially calculated by applying the method from the Brunauer−Emmet−Teller theory (A_{BET}),[22] but these values were discarded because of inconsistencies in the BET c constant; especially, c negative values and values much higher than 200. The method derived from χ-theory was thus applied for determining the surface area (A_χ).[23] The latter was found to agree well with estimations from the α-s method[24] (see Supporting Information). Pore size distributions were calculated by the Barrett−Joyner−Halenda (BJH) method.[25]

The N_2 adsorption−desorption isotherm of graphite (see Supporting Information) showed no apparent hysteresis, and its shape corresponded to Type II in the IUPAC classification,[26] say the graphite used here was basically nonporous or macroporous. Figure 1 features the N_2 adsorption−desorption isotherms for selected VAlO-NC-NT (Figure 1a), VAlO-C (Figure 1b), VAlO-3G-NC (Figure 1c), and VAlO-3G-C (Figure 1d) catalysts. The rest of the isotherms are available on the Supporting Information. All isotherms were Type IV and did not reach a plateau at the high-pressure range ($P/P_0 > 0.9$) which is indicative of H3 hysteresis.[26]

Table 1 presents A_χ of graphite, VAlO-NC-NT, VAlO-C-NT particles, and VAlO-xG-NC/C particles recovered after

Table 1. Surface Area of VAlO-xG-NC/C Catalysts As Determined from Chi (χ) Theory[23] and Cumulative Mesopore Volume and Mesopore Area of VAlO-xG-NC/C Catalysts from the Adsorption Branch of the N_2 Isotherm As Calculated by BJH Method[25] for Slit-Shaped Pores^a

catalyst	A_χ (m^2/g)	adsorption BJH $\sum V_p$ [cm^3/g]	adsorption BJH $\sum S_p$ [m^2/g]
graphite	9	N.D.	N.D.
VAlO-NC-NT	156	0.37	123
VAlO-NC	108	0.24	80
VAlO-C-NT	161	0.39	130
VAlO-C	111	0.3	97
VAlO-1G-NC	77	0.23	57
VAlO-1G-C	28	0.14	35
VAlO-3G-NC	94	0.18	67
VAlO-3G-C	35	0.15	37
VAlO-7G-NC	91	0.19	69
VAlO-7G-C	100	0.26	109

^{a} x = graphite nominal content; NC = non-calcined; C = calcined; N.D. = not determined; N.T. = not tableted.

crushing the corresponding tablets. A_χ of graphite was determined to be 9 m^2/g. On the other hand, important changes in surface area were registered after tableting and after calcination. Compared to the surface area of the VAlO-NC-NT reference (A_χ = 156 m^2/g) the tableted VAlO-NC hydroxide lost 31% in surface area. Conversely, calcination of the reference slightly increased its surface area (A_χ = 161 m^2/g for VAlO-C-NT). The A_χ surface area changed with graphite loading for both the noncalcined and the calcined VAlO-xG-NC/C catalysts. For the noncalcined catalysts, the lowest A_χ

was registered for VAlO-1G-NC (77 m^2/g) which represents a loss of 51% in surface area as compared to the reference. Further increase in graphite loading led to a lower surface area loss; about 40% for both VAlO-3G-NC and VAlO-7G-NC. Moreover, above 3 wt % graphite loading loss in surface area remained constant possibly because of completion of the lubricating layer formed by graphite between the external rim of the tablets (Figure 2) and the machine's pistons walls that leads to the minimum die-wall friction force attainable.[12]
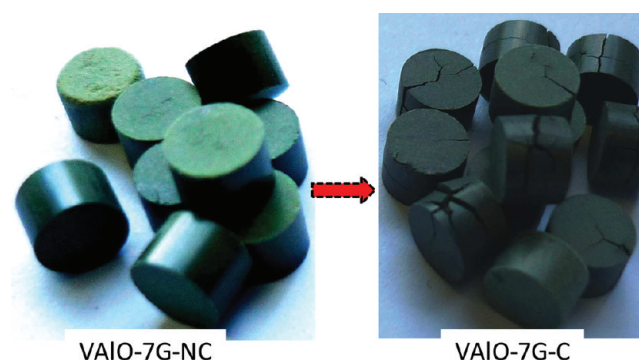

Figure 2. Picture of VAlO-7G before and after calcination.

The surface area of tableted VAlO-xG changed after calcination at 773 K. Further surface area loss was observed (Table 1). Compared to the VAlO-C-NT reference, the tendency in A_χ surface area loss was VAlO-1G-C (83%) > VAlO-3G-C (78%) > VAlO-7G-C (38%) > VAlO-C (31%). The minimum surface area was exhibited for 1 wt % graphite. Comparing the surface area of the catalysts before and after calcination (Table 1), it is noticed that except for VAlO-7G-C all of the noncalcined catalysts exhibited higher surface areas. During calcination the catalysts lost 40 wt % mainly because of water release from the hydroxides. Consequently, extensive cracking of the tablets was observed (Figure 2). One may speculate on the basis of the transformation of the VAlO from a hydroxide into a mixed oxide that this was partly due to growth of particle size caused by the rearrangement of the vanadium−aluminum molecular structure (see Raman results). However, a comparison of the surface areas of VAlO-NC-NT and VAlO-C-NT indicates that graphite is responsible for the observed surface area loss in VAlO-xG-C. Nevertheless, we admit that only a comprehension of the calcination stage can provide a satisfactory explanation on the registered trend in surface area loss reported herein.

Figure 3 displays the BJH pore size distribution, that is, $\delta V_p/\delta\langle w_p\rangle$ as a function of pore width ($\langle w_p\rangle$) as determined from both the adsorption and desorption branches of the physisorption isotherms for selected VAlO and VAlO-3G catalysts, before and after calcination. BJH distribution plots for the other catalysts can be found in the Supporting Information. BJH calculations were performed by considering a slit-shape pore geometry provided by the morphology observed by SEM (Figure 4) and an analysis of the N_2 physisorption data from the works of De Boer et al.[27,28] The shape of the pore distribution curves significantly differed depending on the selected isotherm branch; those coming from the adsorption branch exhibiting clearer peaks. This difference has been ascribed to distinct mechanisms of pore filling and pore emptying.[24,26,28] Because of this, IUPAC recommends only to take into account the adsorption branch of the isotherm to
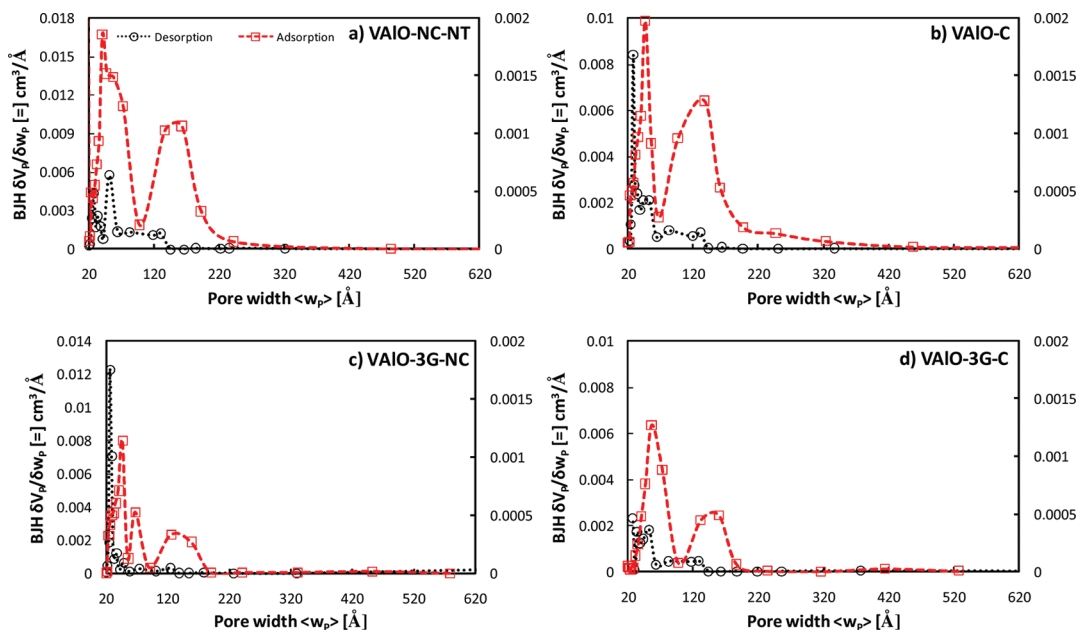
Figure 3. BJH Pore size distribution of selected VAlO-xG-NC/C catalysts: (a) VAlO-NC-NT; (b) VAlO-C; (c) VAlO-3G-NC; (d) VAlO-3G-C.
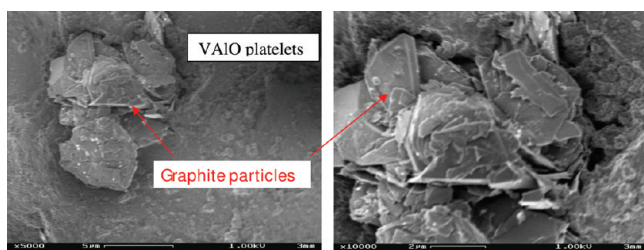

Figure 4. SEM micrographs of a selected VAlO-xG catalyst.

assess the pore size distribution of this type of materials.[26] Consequently, calculations from the desorption branch were discarded. VAlO-NC-NT (Figure 3a) displayed two peaks, the first between 22−99 Å with a salient peak at 40 Å followed by a shoulder at 56 Å, and the second from 99−242 Å centered at 148 Å. The shape of the first peak was changed for VAlO-C (Figure 3b) by becoming very sharp and centered at 45 Å. Moreover, both peaks positively shifted from the positions registered for VAlO-NC-NT to the ranges 23−68 Å and 68−320 Å, respectively. For VAlO-3G-NC, three peaks in the ranges 22−55 Å, 55−92 Å, and 92−192 Å, with centers at 29, 68, and 127 Å, respectively, were registered after calcination. These peaks evolved into two peaks located at 28−98 Å, and 98−190 Å. Though the above trends did not follow a straightforward correspondence with graphite loading, shifts to larger $\langle w_p \rangle$ values were consistently observed after shaping.

Table 1 presents the BJH cumulative mesopore volume ($\sum V_p$) and the cumulative mesopore surface area ($\sum S_p$) for VAlO-NC-NT, VAlO-C-NT, and for VAlO-xG-NC/C samples. $\sum S_p$ of the samples was always lower than the total surface of the materials, which is normal when one performs this kind of calculations.[24,26−28] There was a decrease in $\sum V_p$ after tableting the VAlO-NC hydroxide ($\sum V_p$ = 0.37 cm^3/g for VAlO-NC-NT; $\sum V_p$ = 0.24 cm^3/g for VAlO-NC). Conversely, calcination of pure VAlO samples had a slightly positive effect on $\sum V_p$, more precisely: VAlO-NC-NT ≤ VAlO-C-NT (0.39 cm^3/g), and $\sum V_p$ for VAlO-NC ≤ $\sum V_p$ for VAlO-C (0.30 cm^3/g). In regard to graphite loading, $\sum V_p$ for VAlO-xG-NC followed the

trend VAlO-1G-NC (0.23 cm^3/g) > VAlO-3G-NC (0.18 cm^3/g) ≥ VAlO-7G-NC (0.19 cm^3/g). Accordingly, no significant difference between $\sum V_p$ for VAlO-NC and VAlO-1G-NC was detected, but further increase in graphite loading decreased $\sum V_p$ nonetheless. One must take into account that the BJH method only assesses the total volume of mesopores.[25] Slit-shaped pores are typical of materials composed by plate like particles which is the actual case of both graphite[12] and VAlO (see Figure 4). Considering that the force applied on the VAlO-xG materials during tableting is perpendicular to these particles, one can easily envisage that during powder pressing particles break one against each other, thus reducing interstitial voids and at the same time exerting significant pressure on pore walls either causing pore collapsing or widening. Therefore, an augmentation in the number of micro- and/or macropores should be indeed observed. One advantage of χ-plots is that they are standard isotherms by themselves thus helping to identify qualitative characteristics of the porous structure. In particular, a nonzero interception over the y-axis is indicative of microporosity.[23] Inspection of χ-plots of the samples (see Supporting Information) leads the conclusion that though VAlO-xG-NC/C catalysts possess a certain fraction of micropores, their relative quantity did not increase for none of the samples as compared to VAlO-NC-NT. An additional comparison made with the nonporous alumina standard isotherm led to a similar conclusion. Considering these facts, tableting of VAlO-xG hydroxides conducts to pore widening; hence the mesopores of VAlO-xG become macropores. This latter conjecture is consistent with the trends observed in the BJH distribution presented in Figure 3 and with the decrease in total surface area.

The positive effect of calcination on the cumulative mesopore volume of the pure VAlO materials was not observed for VAlO-xG-C. The cumulative mesopore volume for the calcined catalysts followed the trend VAlO-7G-C (0.26 cm^3/g) > VAlO-3G-C (0.15 cm^3/g) ≥ VAlO-1G-C (0.14 cm^3/g). The tendency in $\sum V_p$ for this group of samples agrees with the previous observations concerning the role of graphite in surface area loss. In addition to what has already been said one must

notice that the catalyst containing the highest graphite loading (VAlO-7G) was the one that lost less surface area, being in addition the one that increased its mesopore volume after calcination the most (Table 1). A hypothesis that could explain such particular behavior is the opening of new mesopores in the graphite particles themselves because of water release from the VAlO hydroxide rather than extensive pore widening of the main VAlO hydroxide structure as observed for lower graphite loading. Water interaction and adsorption on graphitic materials was thoroughly studied by Morimoto and Miura[29,30] during the 1980s. They established that once water chemisorbs on the slit shaped pores of graphite, as it is the case when the graphene layers are oxidized by −OH groups, it accelerates further physisorption of water on the graphite pores. Recently published results on the formation of phenol groups on the surface of hydrated graphite oxide[31] demonstrated that the insertion of a water layer in the basal spacing between graphene layers occurs. The extensive cracking of the VAlO-7G-C tablets (Figure 2) attests for the violence with which water release from VAlO dehydroxylation occurred. A modification of graphite's surface can be certainly expected from this phenomenon.

3.2. Mechanical Resistance of VAlO-xG-NC Tablets.
The mechanical strength of the tableted VAlO-xG hydroxides was evaluated in terms of their compressive strength resistance (σ_ε). Figure 5 features σ_ε as a function of graphite loading.
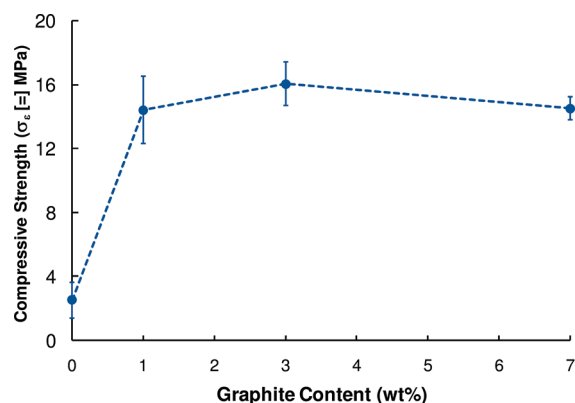

Figure 5. Compressive strength of tableted VAlO-xG catalysts. Error bars correspond to the standard deviation of the data.

Plotted σ_ε values correspond to the average of at least five measurements in the mechanical resistance machine. The mechanical strength of the VAlO-xG-NC tablets was boosted by graphite. Pure VAlO-NC tablets displayed an average σ_ε of about 2.5 MPa, whereas the average σ_ε for VAlO-1G-NC was 14.5 MPa. The three catalysts displayed almost the same average σ_ε values, showing that graphite's positive effect on compressive strength did not depend on its loading. These results are in good agreement with those previously reported for graphite tableted bismuth molybdate (BiMo-xG) catalysts.[12] An explanation was provided considering the resistance of the graphene layers to perpendicular forces; as it is the case of the forces applied to the samples during the compressive resistance tests. In this case, the fact that VAlO particles have a plate-like morphology (Figure 4) can be considered to be an additional factor favoring a strongest enhancement of this mechanical property as compared to BiMo-xG catalysts: σ_ε values for BiMo-xG materials were 3 times higher as that of pure BiMo,[12] whereas the enhancement for VAlO-xGs was about 7 times.

3.3. Surface Chemical Properties of VAlO-xG-NC/C Catalysts.
The surface chemical properties of the materials were determined by XPS. Table 2 shows the surface elemental composition of VAlO-xG-NC/C before and after the catalytic tests. The (V+Al)/O ratio was approximately constant for the noncalcined samples ($0.40 \leq (V+Al)/O \leq 0.43$) and increased after calcination ($0.51 \leq (V+Al)/O \leq 0.56$). For the spent catalysts, this ratio was also rather constant. The surface concentration of metallic atoms did not depend on graphite loading. The increase in the surface concentration of the metals after calcination is related to the abundant loss of water from the VAlO hydroxides during calcination. Concerning carbon concentration, the C/(V+Al+O) atomic ratio expectedly increased with graphite loading but did not markedly change after calcination. The C/(V+Al+O) ratio of the spent catalysts displayed the same qualitative trend, but its values were lower as compared to fresh VAlO-xG-NC/C. The fact that the latter trend did not depend on the presence of graphite, that is, the same was registered for pure VAlO-NC/C, for example, VAlO-NC-NT (C/(V+Al+O) = 0.21) and spent VAlO-NC-NT (C/(V+Al+O) = 0.12), suggests that graphite was not burned into CO_x under reaction conditions. These results suggest that graphite is stable under the oxidative conditions employed in this work.

To discern the oxidation state of the analyzed elements, the binding energy scale was set in respect to the Al 2p peak located at 74.5 eV. This peak was preferred over the C—(C,H) adventitious carbon because of the overlapping of the contamination carbon peak and the graphite peak.[12] Table 3 presents results from the fitting of the C 1s peak of the samples. For VAlO-NC-NT, VAlO-NC, VAlO-C-NT, and VAlO-C the following species were identified: (i) C—(C,H) from hydrocarbons (BE = 284.8 eV); (ii) C−OH alcohol functional group (BE = 286.3 eV); (iii) O−C−O plus C═O from (hemi)acetal and aldehyde functional groups (BE = 287.8 eV); and, (iv) (C═O)−OH plus (C═O)−O−C from carboxyl and ester functional groups (BE = 289.1 eV). In this fitting the same fwhm for all components was assumed, and the binding energy gap between C—(C,H) and C−OH components was fixed at 1.5 eV.[19] The relative concentration of the four carbon species was approximately similar for VAlO-NC-NT, VAlO-NC (not shown) and VAlO-C and VAlO-C-NT (not shown), more precisely, about 70% for C—(C,H), 13% for C−OH, 7% for [O−C−O, C═O], and, 10% for [(C═O)−OH, (C═O)−O-C]. This relative distribution was independent of the total carbon surface concentration which was found to decrease after calcination (see Table 3). To decompose the C 1s peak of the VAlO-xG samples, the graphitic component (C−C) was taken directly from the C 1s peak of an XPS spectrum of the graphite used here.[12] This methodology was proven successful in the XPS analysis of BiMo-xG.[12] Figure 6 shows the fitting of the C 1s line for (a, b) VAlO-NC/C, (c, d) VAlO-1G-NC/C, (e, f) VAlO-3G-NC/C, and, (g, h) VAlO-7G-NC/C. No additional constraints other than those previously imposed for the fitting of C 1s in pure VAlOs were imposed. The results presented in Figure 6 demonstrate that C 1s peak becomes asymmetrical with graphite loading. In general, the C−C component was located in the range 283.0−283.4 eV. The first component of carbon contamination was determined to be between 284.7−285.0 eV thus corresponding to hydrocarbon C—(C,H). Accordingly, the second component was supposed to correspond to C−OH and thus its position was assumed to be at 1.5 eV from C—(C,H), that is, BE = 286.3−286.5 eV.

Table 2. XPS Surface Chemical Composition of Fresh and Spent VAlO-xG-NC/C Catalysts

catalyst	atomic %					atomic ratios	
	carbon	oxygen	vanadium	aluminum	nitrogen	(V+Al)/O	C/(O+Al+V)
				Fresh Catalysts			
VAlO-NC-NT	17.1	57.0	2.8	21.3	1.7	0.42	0.21
VAlO-1G-NC	23.4	52.5	2.6	19.9	1.7	0.43	0.31
VAlO-3G-NC	25.1	51.5	2.5	19.2	1.7	0.42	0.34
VAlO-7G-NC	31.0	48.4	2.4	16.9	1.5	0.4	0.46
VAlO-C	13.7	55.6	4.6	25.8	0.3	0.55	0.16
VAlO-1G-C	19.6	51.3	3.5	25.3	0.3	0.56	0.24
VAlO-3G-C	24.2	48.9	3.2	23.5	0.1	0.55	0.32
VAlO-7G-C	33.8	43.7	3.1	19.1	0.3	0.51	0.51
				Spent Catalysts			
VAlO-NC-NT	10.5	62.0	5.1	21.5	1.0	0.43	0.12
VAlO-1G-NC	12.3	59.4	4.5	22.7	1.0	0.46	0.14
VAlO-3G-NC	22.6	54.1	4.2	18.4	0.8	0.42	0.29
VAlO-7G-NC	25.9	51.5	4.1	17.3	1.1	0.42	0.35
VAlO-C	10.6	61.6	4.5	22.3	1.0	0.44	0.12
VAlO-1G-C	12.7	59.7	4.7	22.0	0.8	0.45	0.15
VAlO-3G-C	16.2	58.2	4.4	20.3	0.9	0.43	0.20
VAlO-7G-C	24.6	51.3	3.9	19.2	1.0	0.45	0.33

Table 3. Relative Concentration of the Components of the C 1s Peak of VAlO-xG-NC/C Catalysts from XPS

catalyst	atomic %					
	C−C graphite	C−(C,H)	C−OH	C=O; O−C−O	(C=O)−OH; (C=O)−O−C	C−C/org. carbon[b]
VAlO-NC-NT	0.0	70.8	12.6	5.3	11.2	0
VAlO-C	0.0	70.0	14.1	6.3	9.6	0
VAlO-1G-NC	23.2	46.2	20.4	5.0	5.2	0.30
VAlO-3G-NC	19.9	54.0	13.2	3.0	9.9	0.25
VAlO-7G-NC	45.0[a]	34.1	10.9	5.9	4.1	0.82
VAlO-1G-C	18.2	55.8	12.0	5.7	8.3	0.22
VAlO-3G-C	26.6	52.8	6.4	5.3	8.8	0.36
VAlO-7G-C	77.5	12.3	7.1	1.3	1.9	3.44

[a]This value was calculated from the sum of the carbon component at 282.1 eV plus C−C graphite. [b]Organic carbon = C−(C,H) + (C−OH) + [C=O, O−C−O] + [(C=O)−OH, (C=O)−O-C].

The third component of adventitious carbon was found to be located at 288.3 eV for VAlO-xG-NC and between 287.5−288.1 eV for all VAlO-xG-C catalysts. In spite of the lower binding energy of the latter, this component still probably corresponds to [O−C−O, C=O] species. A fourth carbon component was determined to be at 289.0−289.3 eV, with no particular differences between the noncalcined and calcined VAlO-xG samples. Therefore, this component was assigned to [(C=O)−OH, (C=O)−O-C] plus the π−π shakeup of graphite.[32] The C 1s peak of VAlO-7G-NC displayed an additional component located at 282.1 eV. According to literature,[33−36] such component corresponds to a carbon−metal bonding in carbide species, and it is most probably an impurity in graphite.[37] The fact that it was only present for the noncalcined sample with the highest graphite loading suggests that its concentration is very low and, in addition, that it can be easy eliminated from the catalyst's surface.

The position of the graphite C−C component in VAlO-xG agrees with several literature reports.[33−35,38,39] Weckhuysen et al.[35] and Wang et al.[39] investigated the nature of the carbon species present on the surface of zeolite supported molybdenum catalysts (Mo/H-ZSM-5) for alkane dehydroaromatization. Both groups independently reported a BE of 283.2 eV for graphitic carbon species when using the zeolitic Al 2p peak as a reference to fix the binding energy scale. On the basis

that this carbon species was formed after exposure of the Mo/H-ZSM-5 catalyst to a CO flow at 993 K, Weckhuysen et al.[35] suggested that this graphitic carbon was a hydrogen-poor sp-type carbon species of rather amorphous nature and hence called it *pregraphitic-like*. On the other hand, Bismarck et al.[38] studied the effect of fluorination of highly oriented pyrolytic graphite fibers to increase the surface polarity of their carbon atoms. They found that the position of the C 1s peak shifted from 284.8 to 283.3 eV when attacking one of the fibers with the highest fluorine concentration. This in turn resulted in lower electrical conductivity which they suggested was due to a transformation of the sp[2] orbitals of the π-aromatic bonds of graphite into sp[3] orbitals from ionic fluorocarbon-graphitic bonds.[38] It is interesting to notice that these authors[38] carried out their XPS analyses using an aluminum sample holder and that they decomposed the C 1s peak without fixing the position of the graphite C−C component. In this respect, their strategy for data treatment was similar to the one adopted herein. On the other hand, the binding energy of the graphite C−C component of VAlO-xG differs from the value found for BiMo-xG, the latter being at 284.5 eV.[12] In that case, the binding energy was found to be in correspondence with the main symmetric component used in the fitting of the C 1s peak of highly oriented pyrolytic graphite (HPOG) proposed by Blyth et al.[36] The fitting methodology used by these authors was
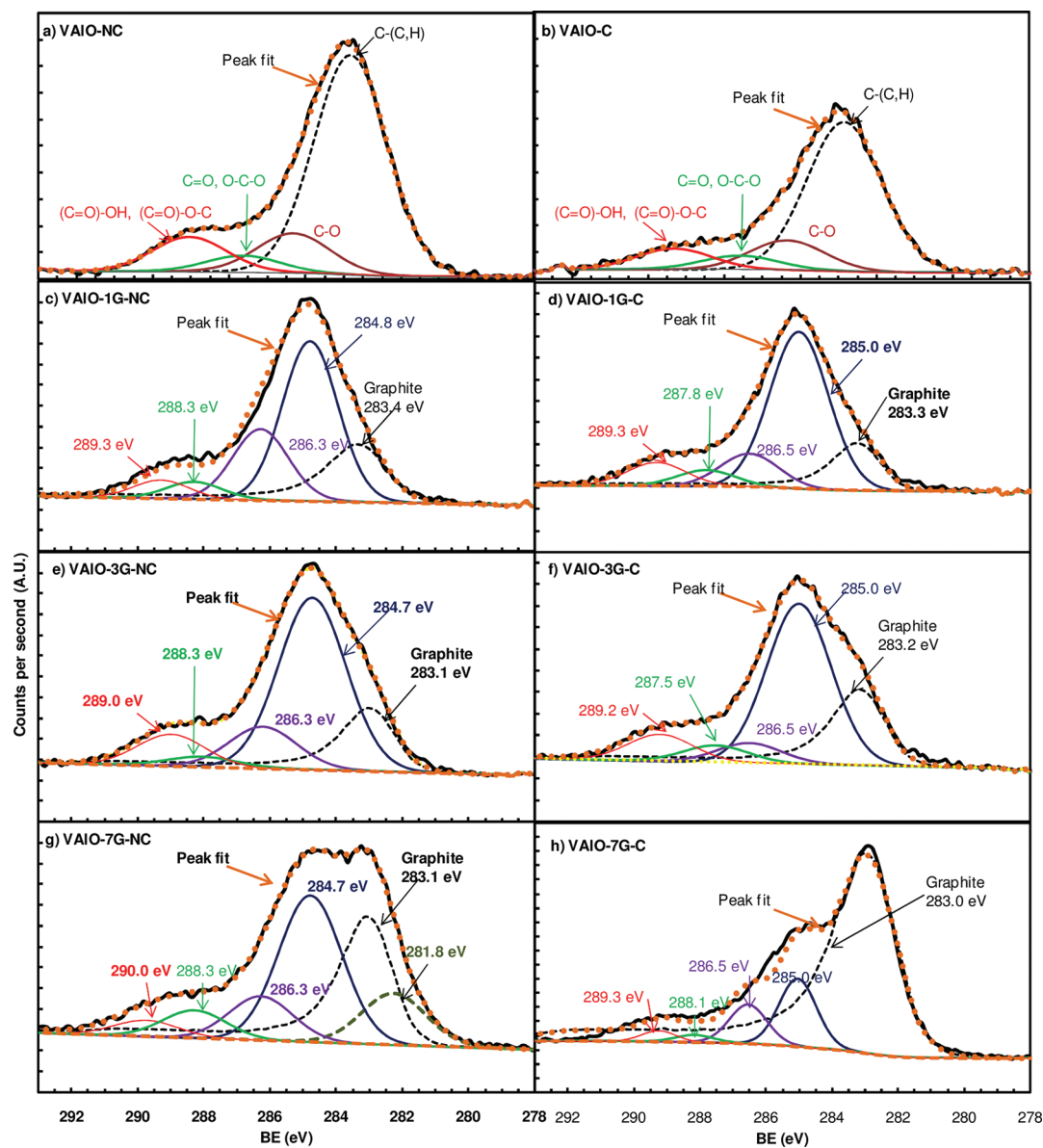
Figure 6. Fitting of the C 1s peak of VAlO-*x*G-NC/C catalysts.

based on the assumption that the asymmetry of the graphite C 1s peak can be accounted from the individual contributions of the C−C component at 284.4 eV and the contribution from the hydrocarbon C—(C,H) contamination. The assignment of the BE of the graphite C−C contribution was taken from the position of the C 1s peak of HPOG reported in the early works of van Attekum et al.[40] and Sette et al.[41] who did not performed a fitting of the peak but rather aimed at understanding the nature of the asymmetry of the peak. Nevertheless, this does not explain why the BE of the graphite C−C component of VAlO-*x*G shifted with respect to BiMo-*x*G.[12] Sette et al.[41] concluded that the most interesting observation of their work was the high sensitivity of the width of the C 1s peak to the chemical environment. Furthermore, controlling the electronic properties of graphene layers through a comprehension of their molecular interactions with diverse substrates is a very hot topic in materials science.[42,43] It has been found that the intrinsic electronic properties of separated graphene layers are drastically modified because of the molecular disorder induced by its interaction with SiO$_2$ substrates.[42] The graphite used in our

research is constituted by a combination of amorphous and crystalline graphene layers.[12] Considering the above arguments it thus seems reasonable to ascribe the difference in the position of the graphite C−C component between BiMo-*x*G and VAlO-*x*G to electrical conductivity effects induced by the interaction of graphite with these two different materials. Charging effects leading to spectrum misinterpretation were completely ruled out during the experiments and reproducibility of the measurements was verified. Additional support to this hypothesis is the fact that bismuth molybdates are semi-conductors[44] whereas parent alumina (hydr)oxides constituting most of the VAlO structure (see Raman section) are strong insulators.[45] It must be admitted though that the fitting of the C 1s peak of the VAlO-*x*G-NC/C samples proposed here has its own limitations, mainly because the direct insertion of the C 1s peak of graphite into the model can already include contributions from hydrocarbon C−[C,H] and oxygen functionalities present on graphite surface. Therefore, a straightforward quantitative interpretation of the data can be risky but does not impede a proper qualitative evaluation of the

Table 4. Relative Concentration of the Components of the C 1s Peak of VAlO-xG-NC/C Catalysts from XPS

catalyst	V 2p$_{3/2}$			O 1s		
	V^{5+}	V^{4+}	V^{5+}/(V^{5+}+V^{4+})	V−O−Al	O−H, O−C	V−O−Al/[V−O−Al + O−H, O−C]
VAlO-NC-NT	2.1	0.7	0.75	13.5	43.5	0.24
VAlO-1G-NC	2.0	0.6	0.76	16.1	36.4	0.31
VAlO-3G-NC	2.1	0.4	0.83	10.2	41.2	0.20
VAlO-7G-NC	2.2	0.1	0.96	9.3	39.0	0.19
VAlO-C	3.3	1.3	0.72	33.8	21.8	0.61
VAlO-1G-C	2.6	0.9	0.74	34.0	17.3	0.66
VAlO-3G-C	2.7	0.5	0.84	22.4	26.6	0.46
VAlO-7G-C	2.3	0.9	0.72	23.6	20.1	0.54

observed trends. In this sense, results concerning the graphite C−C to organic contamination ratios presented in Table 3 are consistent with an increase of the relative concentration of the C−C component with graphite loading. For VAlO-7G-NC it was considered that the component at 282.1 eV was rather associated to graphitic carbon; hence, the value for the C−C component presented in Table 3 corresponds to the sum of the atomic percentage of this component plus the original graphite C−C component. Among the noncalcined catalysts, the aforementioned increase in graphite C−C concentration was stronger for VAlO-7G-NC and became remarkably stronger after calcination (graphite C−C/organic carbon ratio = 3.44). Notice how the line shape of the C 1s peak of VAlO-7G-NC (Figure 6g) is comparatively more complex than for the other samples in Figure 6 and how it became very sharp after calcination thus resembling that of pure graphite.[12]

The ensemble of the results and discussion featured above evidence that no straightforward interpretation of the C 1s XPS line of carbon in graphite containing catalytic powders is attainable. Careful fitting of the peak must take into account the contribution of surface carbon species linked to both adventitious carbon contamination and graphite. Moreover, the difference in electronic conductivity between graphite and the catalytic powder determined the binding energy of the graphite C−C component employed during peak fitting. A comparison of the results obtained for the noncalcined and calcined VAlO-7G-NC/C catalyst suggests that a more intimate surface electronic interaction is present between graphite particles and VAlO (Figure 6).

A single region between 508.6−538.6 eV was used to analyze the V 2p$_{3/2}$ and the O 1s peaks of the catalysts. The V 2p$_{3/2}$ peak was decomposed into a component at 517.5−517.8 eV ascribed to the V^{5+} oxidation state and another one at 516.0−516.8 eV ascribed to V^{4+}.[33,34,36] The O 1s peak of the samples was decomposed into a component ascribed to oxygen bonded to vanadium and aluminum (called herein V−O−Al) located in the range 530.4−530.8 eV and another ascribed to oxygen bonded to hydroxyl −OH and carbon groups (O−[C,OH]).[46] An examination of the O 1s plus V 2p$_{3/2}$ region for VAlO-xG-NC/C (not shown) indicated that neither calcination nor graphite caused a strong binding energy shift in V 2p$_{3/2}$. Table 4 presents the relative distribution of the vanadium and oxygen species according to the fitting of the studied XPS peaks. The fwhm of the components of the V 2p$_{3/2}$ peak were in the range 2.1−2.9 eV. The noncalcined catalysts showed a sustained tendency to an increase in the V^{5+}/(V^{5+} + V^{4+}) ratio with graphite loading. Such trend was not observed for the calcined samples. A maximum in V^{5+}/(V^{5+} + V^{4+}) ratio was registered for VAlO-3G-C whereas this ratio remained rather constant for the other samples. Though the above-described results are

numerically and qualitatively consistent, one must be careful when drawing definite conclusions regarding the oxidation state of vanadium of VAlO because these materials have displayed a certain susceptibility to reduction by the X-ray beam of the apparatus.[47] Nevertheless, given the uniformity in the conditions of the present analyses the described trends can be certainly considered to be qualitatively valid. In this regard, the present XPS results allow concluding that the majority of the vanadium surface species in VAlO-xG-NC/C corresponds to the V^{5+} oxidation state. Indeed, previous X-ray absorption spectroscopy (XAS) measurements performed on noncalcined VAlO[48] showed that vanadium has an estimated valence of 5.5+. Nevertheless, for the current study the presence of a certain concentration of V^{4+} species in VAlO-xG-NC/C cannot be ruled out.

Calcination increased the concentration of oxygen species ascribed to V−O−Al (Table 4). Indeed, a 2- to 3-fold increase in the V−O−Al/(V−O−Al + [O−H, O−C]) ratio of the samples was determined after calcination. Such change was accompanied by a modification of the symmetry of the O 1s peak and a shift of about 0.7 eV to lower binding energy (not shown). The enrichment in V−O−Al did not follow a straightforward relationship with graphite loading. The structural transformation of the vanadium−aluminum hydroxide into a mixed oxide is related to this trend. Numerous surface O−H groups are eliminated during the process as it was evidenced by the weight loss of the calcined catalysts (average weight loss = 33.5 wt %). The results obtained in the fitting of the C 1s peak (Table 3) indicate that the decrease in the concentration of carbon bonded oxygen surface species was not as important as to be taken into account to explain the phenomenon.

Residual nitrogen from VAlO hydroxide synthesis was also found in XPS analysis (Table 2). A part of the residual nitrogen was found to survive calcination, more precisely the one corresponding to NH$_x$[33,34] species (BE = 400.2 eV),[32,33] whereas the one ascribed to NO$_3$ species[33,34] (BE = 407.2 eV) was not detected in the calcined catalysts.

Finally, it must be mentioned that a very wide peak was always registered at 71 eV, that is, next to the Al 2p peak. This peak was ascribed to V 3s and is due to the high concentration of vanadium in the bulk mixed (hydr)oxides.

3.4. Molecular Structure of VAlO-xG-NC/C Catalysts. Raman technique provided evidence on the molecular conformation of the structure of the VAlO-xG materials and also on the evolution of such structure during calcination.

VAlO materials are part of the family of transition metal vanadate of general chemical formula Al$_x$V$_6$O$_{13+y}$. The internal molecular arrangement of the structure is quite complicated and depends strongly on the distribution of aqueous vanadate

and aluminate species during synthesis.[13,49,50] In particular, under the synthesis conditions used here, pH = 5.5 and [V] = 0.030M, a mixture of $H_xV_{10}O_{28}^{6-}$ decavanadates and $[AlO_4Al_{12}(OH)_{24}(OH_2)_{12}]^{7+}$ aluminum amorphous aqueous species are precursors to the precipitated hydroxide. Figure 7 presents the
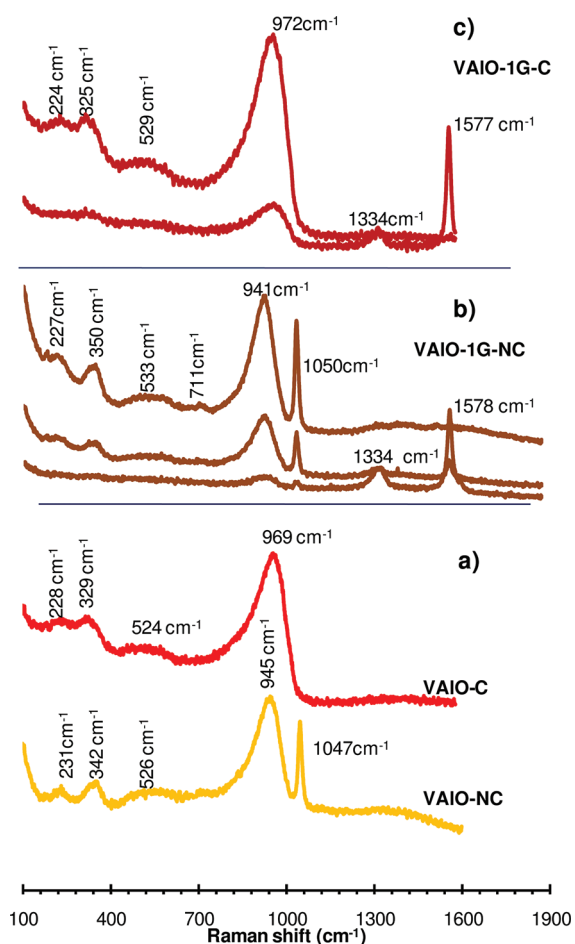

Figure 7. Raman spectra of selected VAlO-xG-NC/C: (a) Pure VAlO before and after calcination; (b) Spectra registered for three different particles of VAlO-1G-NC; and (c) spectra recorded for two different particles of VAlO-1G-C.

Raman spectra of selected VAlO-NC and VAlO-C (Figure 7a), VAlO-1G-NC (Figure 7b), and VAlO-1G-C (Figure 7c) as taken at ambient conditions. Raman spectra of the other catalysts presented similar characteristics. Noncalcined VAlO-NC (Figure 7a) exhibited bands at 231, 342, 945, and 1047 cm^{-1} besides a shoulder at 526 cm^{-1}. Most of these bands had been also detected in VAlO catalysts synthesized at the laboratory scale.[49] Given the bulk nature of the VAlO mixed (hydr)oxides, assignment of these bands is not ambiguity free because bonds from both aluminum and vanadium can vibrate at very close, if not the same, wavenumbers. Consequently, to approach a more realistic image of the molecular structure of VAlO-xG-NC/C it was decided to take both contributions into account for the analysis of these bands. To do so, a literature survey on the Raman spectra and characteristics of pure aluminum (hydr)oxides,[51,52] crystalline aluminum vanadates (AlVO$_4$),[53] alumina supported VOx catalysts,[54−56] and parent laboratory scale prepared VAlOs[49] was required. We will

discuss first the detected bands that can be ascribed to aluminum bonds in the VAlO-xG-NC hydroxides.

Colomban[51] studied the Raman spectra of aluminum hydroxides. According to his work the contribution of aluminum hydroxides to the Raman spectra of VAlO-xG-NC can be described as follows. The bands located at 231 and 342 cm^{-1} are related to vibrations from the internal bonds of γ-$Al(OH)_3$ (gibbsite) and/or AlOOH (γ-AlOOH boehmite and α-AlOOH diaspore). The structure of these oxohydroxides were described as consisting of an AlO_6 octahedra chain made with OH groups in the case of $Al(OH)_3$, and as a slab of corner-shared AlO_4 octahedra in the case of AlOOH.[51] Thus the band at 342 cm^{-1} is characteristic of the bending mode in the Al−O chain (slab) with its associated stretching Al−O modes of the AlO_6 octahedron at 526 cm^{-1}. The latter registered herein as a shoulder (Figure 7a). On the other hand, the band at 231 cm^{-1} is associated to the Al−O bending mode of AlO_4. The assignment of these bands also agrees with the Raman study of Ruan et al.[52] for gibbsite, bayerite (α-$Al(OH)_3$), diaspore, and boehmite. Moreover, some of the five bands registered for VAlO-NC (Figure 7a) also match other bands reported by these authors.[52] This fact sheds more light in the interpretation of the Raman spectra of VAlO-xG-NC. In general, the bands detected by Ruan et al.[52] can be grouped into three major regions: one at 200 to 499 cm^{-1} for vibrations of Al−O bonds, another at 500−899 cm^{-1} for vibrations of $\gamma(OH)$ bonds, and the other at 900−1200 cm^{-1} for vibrations of $\delta(OH)$ bonds. Comparing their results to ours, one can see that the band of VAlO-NC at 231 cm^{-1} was close to one of the bands ascribed to the Al−O vibration in boehmite (228 cm^{-1}) and bayerite (237 cm^{-1}). The shoulder at 526 cm^{-1} of VAlO-NC is in the same region (506−669 cm^{-1}) of the bands registered for the vibration of the $\gamma(OH)$ bonds of diaspore, bayerite, and gibbsite. Actually, in Ruan et al.'s work[52] gibbsite and bayerite most intense bands associated with Al−O−Al bonds were registered in this region. The strongest band of VAlO-NC at 945 cm^{-1} is near to the broad and weak 956 cm^{-1} band of $\delta(OH)$ vibration, that is, an Al(OH) bending mode, in diaspore. Finally, the sharp VAlO-NC band at 1047 cm^{-1} coincides with weak bands at 1051 cm^{-1} and 1045 cm^{-1} recorded for the vibration of $\gamma(OH)$ in gibbsite and bayerite, respectively.[52] Considering the above comparison one may suggest that aluminum is simultaneously conforming both $Al(OH)_3$ and AlOOH structures in VAlO-xG-NC with $Al(OH)_3$ and AlOOH being highly hydrated amorphous phases. This is additionally supported by the fact that VAlO-xG-NC hydroxides were only dried at 333 K during the study. Moreover VAlOs are amorphous,[49] and, as said before, lost about 33.5 wt % during calcination which is much more than the theoretical water loss of boehmite for example.[57]
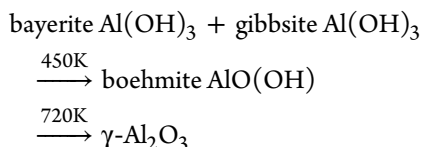
Concerning the contribution of vanadium species to the Raman spectra of VAlO-xG-NC, the bands centered at 945 cm^{-1} and 1047 cm^{-1} of VAlO-NC are very distinctive of vanadium bonding in crystalline AlVO$_4$ and VO$_x$/Al$_2$O$_3$ catalysts. Most authors[54−56] investigating the properties of VO$_x$/Al$_2$O$_3$ catalysts base their interpretation of Raman spectra on the spectrum of crystalline AlVO$_4$.[53] By extension of such approach, Florea et al.[49] proposed that the presence of bands in the region 940−980 cm^{-1} in the Raman spectra of noncalcined VAlOs correspond to polymeric decavanadate $[V_{10}O_{28}]^{(6-n)-}$ and $[(VO_3)_n]_n$ metavanadate species, whereas the band at about 1050 cm^{-1} is due to monomeric isolated vanadyl species.[54] This interpretation was further supported by XAS measurements[48]

that allow establishing the existence of tetrahedral VO_4 coordination sites with two V=O vanadyl bonds at 1.62 and 1.67 Å and two V—O bonds at 1.80 Å. Nevertheless, the development of UV-Raman spectroscopy has opened a debate on the correctness of the assignment of these bands.[55] The comparison of the changes registered in Raman spectra of silica and alumina supported vanadium catalysts measured with visible (488 nm) and ultraviolet (233 nm) laser excitation with theoretical model studies led to the conclusion that the band at 950 cm^{-1} can be the result of interface V—O—Al interactions and isolated plus polymeric species.[55] In addition, the 1050 cm^{-1} band cannot be solely ascribed to isolated vanadyl species but rather to cluster vanadyl species associated with monomeric and polymeric groups as well as to their bonding to surface oxygens with 2-fold and 3-fold coordinations.

On the other hand, vibrations of V—O—Al bonds have also been registered at short wavenumbers, namely, 226, 329, and 521 cm^{-1}.[53] These bands are near to the low intensity bands recorded for VAlO-NC at 231, 342, 526 cm^{-1} (Figure 7).

The conjunction of all of the above structures on the vanadium−aluminum mixed hydroxide depicts a highly complex heterogeneous material. Though a minute description of its molecular structure of the VAlO-NC materials synthesized here escapes the scope of this paper, a new interpretation of their Raman spectra, beyond the one presented in previous works,[49] can be provided as follows: (i) The aluminum in VAlO-NC simultaneously exists as both $Al(OH)_3$ and $AlOOH$ amorphous phases. Of the two possible polymorphs of $Al(OH)_3$, gibbsite and bayerite, the latter is the one that exhibits Raman bands closer to the 231 and 526 cm^{-1} bands of VAlO-NC at 235 and 525 cm^{-1}, respectively. In addition, the band at 1047 cm^{-1} coincides with that of gibbsite. Regarding the AlOOH phases, they were found to be more akin to diaspore (α-AlOOH) than to boehmite (γ-AlOOH). (ii) Vanadium is conforming polymeric decavanadate $[V_{10}O_{28}]^{(6-n)}$, $[(VO_3)_n]_n$ metavanadate, and, isolated and cluster vanadyl species. (iii) There is evidence on the formation of bridging V—O—Al bonds.

The Raman spectra of the calcined VAlO-C catalyst showed important changes in regard to noncalcined VAlO-NC (Figure 7a). Particularly, the bands at 231 cm^{-1} and 342 cm^{-1} shifted to lower wavenumbers and became less separated. The strongest band at 945 cm^{-1} was displaced to 969 cm^{-1}, and the sharp band at 1047 cm^{-1} disappeared. These changes can be ascribed to the thermal transition of VAlO hydroxide into VAlO mixed-oxide. Aluminum hydroxides go through the following phase transitions:[58]

$$\text{bayerite } Al(OH)_3 + \text{gibbsite } Al(OH)_3$$

$$\xrightarrow{450K} \text{boehmite } AlO(OH)$$

$$\xrightarrow{720K} \gamma\text{-}Al_2O_3$$

Accordingly, calcination at 773 K can theoretically transform all aluminum hydroxides into γ-Al_2O_3. It is thus reasonable to suppose that the aluminum hydroxide species of VAlO-NC undergo a similar phase transformation into a structure resembling that of γ-Al_2O_3. Therefore, it can be considered that the calcined VAlO resembles a structure in which vanadium species are embedded in a γ-Al_2O_3-like matrix. Of course, this latter structure is better defined, and the force of the bonds between the structural vanadium and the aluminum units should be stronger as compared to the noncalcined

hydroxide. Pure γ-Al_2O_3 does not normally exhibit Raman bands because of the ionic character of the Al−O bond in alumina.[56] Hence, the interpretation of the bands displayed in the Raman spectra of calcined VAlO-C is in principle less ambiguous and should resemble more to those of $AlVO_4$[53] and VO_x/Al_2O_3.[54−56] Therefore, the disappearance of the band at 1047 cm^{-1} is ascribed to the polymerization of the hydroxide structural units of AlO_x and VO_x. Such polymerization entails changes in the interaction between the vanadium and aluminum atoms located at the interface between both molecular structures.[55] In fact XAS measurements performed for the nitridation of VAlO materials after calcination at 773 K demonstrated that during such process the coordination of the vanadium atoms changed from tetrahedral to octahedral.[48] The shift of the band at 945 cm^{-1} to a higher wavenumber (969 cm^{-1}) can be interpreted as a transformation of the metavanadate $[(VO_3)_n]^{n-}$ into decavanadate $[V_{10}O_{28}]^{(6-n)}$ and subsequently into amorphous V_2O_5-like species.[56−58] Given the amorphous character of calcined VAlO-C, it is reasonable to affirm that none of the latter phases exist as an independent well-defined crystalline structure inside the mixed oxide. It is worth mentioning that the above interpretation agrees with observations performed on the evolution of the Raman spectra of VO_x/Al_2O_3 catalysts with vanadium loading.[54,56] Finally, the changes recorded for the bands at short wavenumber 220−350 cm^{-1} may be interpreted as a sign of the strengthening of the V—O—Al bonds of the mixed oxide. Conversely, the shoulder at 526 cm^{-1}, associated to $\gamma(OH)$ bonds in the aluminum lattice of the hydroxide and to vibrations of V—O—Al bonds, remained unchanged after calcination. The latter suggests that calcined VAlO keeps a partially hydrated molecular structure.

The Raman spectra recorded for the calcined VAlO-xG-C materials (Figure 7) is quite similar to that reported for vanadium−aluminum aerogels[59] except for the bands of graphite of the former (Figure 7c). The spectra presented in these two figures for both noncalcined and calcined VAlO-xG-NC/C catalysts were taken from different particles of the samples. The Raman bands described for the pure VAlO-NC/C catalysts remained in the same positions for VAlO-xG-NC/C meaning that the molecular arrangement of the structure of the mixed (hydr)oxide was not affected by the presence of graphite. The changes in the intensity of the Raman bands between each particle reflect the heterogeneity of the particles of shaped VAlO-xG-NC/C catalysts; such heterogeneity consisting on a random distribution of graphite and VAlO particles over the shaped materials. In particular, some of these particles clearly displayed the two bands (1334 and 1577 cm^{-1}) assigned to graphite,[60,61] whereas others did not. Moreover, those particles where the graphite bands were more intense showed weaker vanadium−aluminum bands (Figures 7b and 7c). The bands registered for graphite in VAlO-xG-NC/C correspond to those reported for highly ordered graphite. The one at 1577 cm^{-1}, conventionally known as the G-band, has been attributed to the in-phase vibration of the graphite lattice, and the other at 1334 cm^{-1}, the so-called D-band, ascribed to a weak disorder caused by the graphite edges. It is important to notice that the Raman spectra of the first, as counting from below in Figure 7b, of the particles of VAlO-1G-NC displayed wide D- and G-bands, the second which did not apparently displayed the D-band and the G-band was very sharp, and the third particle did not exhibit any noticeable graphite band except for an apparent shoulder where the D-band should appear. The same kind of difference was registered for calcined VAlO-1G-C (Figure 7c). The

widening of the two bands of graphite has been recurrently observed when the degree of disorder of its structure augments because of an amorphization of the graphite structure. Nevertheless, both the D- and G-bands result from vibration of the sp^2 sites of the carbon−carbon structure; more specifically, the D-band is caused by breathing modes of sp^2 atoms in rings and G-band is the product of the stretching of pairs of the sp^2 atoms in both rings and chains.[62]

To summarize all of the above Raman observations and the interpretation of the structural features of the VAlO-xG-NC/C catalysts, it can be said that VAlO-xG-NC hydroxides are conformed by a mixture of highly hydrated structural units of Al(OH)$_3$ and AlOOH which can be considered as a matrix for polymeric deca- $[V_{10}O_{28}]^{(6−n)}$, metavanadate $[(VO_3)_n]_n$ species with the presence of isolated or clustered vanadyl V=O associated to mono and/or polymeric vanadates. This molecular structure evolves after calcination (VAlO-xG-C) into one in which vanadium species have polymerized to larger decavanadate $[V_{10}O_{28}]^{(6−n)}$ chains and amorphous V$_2$O$_5$-like within a γ-Al$_2$O$_3$ matrix. Two bands typically attributed to carbon−carbon bonds of graphite were detected in the analysis, but no additional bands from carbon bonds were recorded suggesting the absence of insertion of carbon atoms directly into the V−O−Al lattice. Heterogeneity in the relative concentration of the phases and the shaping agent inside VAlO-xG-NC/C particles recovered from the tablets was evidenced as the intensity and number of Raman bands of the samples differed from particle to particle. On the basis of the above description a structural model for VAlO-xG-NC/C materials is suggested in Figure 8.
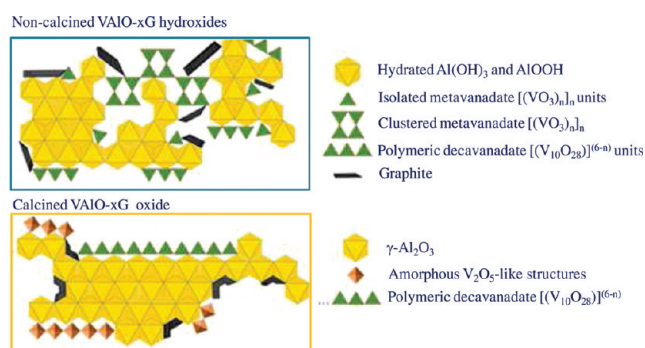

Figure 8. Proposed structural model of VAlO-xG-NC/C materials.

3.5. Catalytic Performance of VAlO-xG-NC/C Materials in Propane Oxidative Dehydrogenation. The catalytic performance of the noncalcined VAlO-xG-NC materials is presented and discussed first, followed by the results obtained for the calcined catalysts. Finally, a comparison of the two series is presented. Considering the N$_2$ physisorption results and the discussion presented in Section 3.1, the intrinsic catalytic activity and yields were normalized using the surface area as determined from the χ-method.

Table 5 shows the steady state catalytic performance of noncalcined VAlO-xG-NC materials in propane oxidative dehydrogenation at 723 and 748 K. At 723 K, the propane catalytic activity for VAlO-xG-NC (a_{C3H8} [m^{-2}]) was rather constant hence not dependent on graphite loading. The corresponding calculated a_{O2} to a_{C3H8} ratio was found to be not higher than 1.6. Regarding selectivity to propene, the most selective catalyst was VAlO-1G-NC (S_{C3H6} = 0.75), whereas the others displayed selectivity values very near to that of pure VAlO-NC. Temperature increase (748 K) augmented propane and oxygen activities. Propane activity at 748 K followed the order VAlO-NC $\approx$ VAlO-1G-NC > VAlO-7G-NC > VAlO-3G-NC. The a_{O2} to a_{C3H8} ratio did not increase in the same order as propane activity. In this case VAlO-NC $\approx$ VAlO-7G-NC > VAlO-1G-NC > VAlO-3G-NC. Selectivity to propene decreased following an inverse trend as that for the increase a_{O2} to a_{C3H8} ratio, with the highest value of 0.53 registered for VAlO-3G-NC. The catalyst that exhibited the strongest selectivity drop was pure VAlO-NC with S_{C3H6} = 0.18, that is, it lost selectivity by a factor of 3 as compared to its value at 723 K (S_{C3H6} = 0.57). Regardless of the considered reaction mechanism[18,54], the stoichiometry of the propane oxidation reaction says that 0.5 mol of molecular oxygen are required for transforming it to propene, C$_3$H$_8$ + 0.5O$_2$ → C$_3$H$_6$ + H$_2$O, whereas 3.5 mols of molecular oxygen are required to achieve complete oxidation of propane into CO$_x$, C$_3$H$_8$ + 3.5O$_2$ → 3CO$_x$ + 4H$_2$O. Solely on this basis, it can be directly deduced why higher oxygen consumption or a_{O2}/a_{C3H8} ratio in the reaction is reflected in lower selectivity to propene. Though the catalytic performance, activity and selectivity, for the non-calcined VAlO-xG-NC did not follow a straight tendency with graphite loading, it is clear that the catalysts containing graphite are more selective to propene at higher temperature, revealing that graphite influences the catalytic functionalities of the vanadium aluminum (hydr)oxides in propane ODH. There is a consensus among the scientific community on the role of V^{5+} species as the most relevant active site for the activation of the propane in ODH reactions.[17,54,62,63] XPS results showed that most of the vanadium in VAlO-xG-NC/C materials is present in such an oxidation state (Section 3.3.) with the presence of a certain fraction of V^{4+} species. So far, the role of the V^{4+} species in the reactivity of alkanes in ODH reactions is not well

Table 5. Steady State Catalytic Performance of Non-Calcined VAlO-xG-NC Materials in Propane Oxidative Dehydrogenation

catalyst	%C_{C3H8}	$a_{C3H8}{}^i$ (m^{-2})	%C_{O2}	$a_{O2}{}^i$ (m^{-2})	a_{O2}/a_{C3H8}	$y_{C3H6}{}^i$ (m^{-2})	$y_{COx}{}^i$ (m^{-2})	S_{C3H6}
				723 K				
VAlO-NC	16.0	0.010	22.1	0.014	1.4	0.006	0.004	0.57
VAlO-1G-NC	10.6	0.013	15.6	0.020	1.5	0.010	0.003	0.75
VAlO-3G-NC	9.6	0.010	10.4	0.010	1.1	0.005	0.005	0.47
VAlO-7G-NC	10.2	0.011	16.0	0.017	1.6	0.005	0.005	0.52
				748 K				
VAlO-NC	47.5	0.030	98.8	0.063	2.1	0.006	0.025	0.18
VAlO-1G-NC	23.1	0.029	39.7	0.050	1.7	0.010	0.018	0.37
VAlO-3G-NC	17.1	0.017	25.3	0.025	1.5	0.009	0.008	0.53
VAlO-7G-NC	23.7	0.024	47.0	0.049	2.0	0.007	0.017	0.31

Table 6. Steady State Catalytic Performance of Calcined VAlO-*x*G-C Materials in Propane Oxidative Dehydrogenation

catalyst	%C_{C3H8}	a_{C3H8}^{i} (m^{-2})	%C_{O2}	a_{O2}^{i} (m^{-2})	a_{O2}/a_{C3H8}	y_{C3H6}^{i} (m^{-2})	y_{COx}^{i} (m^{-2})	S_{C3H6}
				723 K				
VAlO-C	23.7	0.020	54.7	0.046	2.3	0.006	0.014	0.29
VAlO-1G-C	11.0	0.039	35.9	0.128	3.3	0.018	0.025	0.42
VAlO-3G-C	22.2	0.063	37.5	0.106	1.7	0.014	0.031	0.31
VAlO-7G-C	12.7	0.012	34.6	0.033	2.7	0.007	0.005	0.58
				748 K				
VAlO-C	37.6	0.032	98.9	0.084	2.6	0.008	0.025	0.24
VAlO-1G-C	21.5	0.076	72.2	0.257	3.4	0.028	0.046	0.38
VAlO-3G-C	37.0	0.105	90.0	0.255	2.4	0.037	0.057	0.39
VAlO-7G-C	24.3	0.023	73.4	0.069	3.0	0.011	0.012	0.47

established beyond the fact that they seem not to be capable of activating the alkane molecule.[62] Nevertheless, a role of V^{4+} in ODH selectivity should not be discarded. V^{4+} species in multiwalled carbon nanotubes supported VO$_2$ have been found to be more active in benzene hydroxylation than V$_2$O$_5$ because of their better capacity to produce $-$OH radicals from H$_2$O$_2$.[64] Furthermore, it is nowadays recognized that V^{4+} and V^{5+} make part of the active phase of VPO based catalysts for *n*-butane oxidation to maleic anhydride.[65]

Recalling Raman results (Section 3.4.), vanadium in VAlO-*x*G-NCs was found to be present as $[V_{10}O_{28}]^{(6-n)}$ and $[VO_3]^{(6-n)}$ that comprise isolated or clustered V=O species. Klose et al.[62] have proposed a structure for alumina supported VO$_x$/Al$_2$O$_3$ catalysts consisting either of isolated $[V_3O_8]^{3-}$ structures linked by three bonds to the alumina support or polyvanadates composed of chains of $[V_3O_7]^-$ units in which both V^{5+}=O and V^{4+}=O vanadyls are included. In VAlO-*x*G-NC materials these vanadium structures are circumscribed and/or coordinated within a highly hydrated Al(OH)$_3$–AlOOH network. Therefore, the influence of the bonds belonging to the V$-$O$-$Al interface should not be disregarded when discussing the catalytic functionalities of these materials. In fact, Heracleous et al.[66] presented evidence on the reactivity of ethane and ethene over alumina. These authors concluded that hydroxyl ($-$OH) and Al^{3+}-O^{2-} groups are readily able to perform deep oxidation of these hydrocarbons to carbon oxides and coke without necessarily following a redox mechanism. They rather evoked a mechanism via the participation of oxygen active species.[66] Moreover, Schlögl[63] remarked that these hydroxyl groups also play a role in the V^{5+} ↔ V^{4+} ↔ V^{3+} redox dynamics of vanadium. In this work, with the reaction temperature increase, both the catalytic activity and the a_{O2} to a_{C3H8} ratio increased at the expense of the selectivity to propene. It is under these conditions that graphite played the most important role in controlling the functionalities of the vanadium$-$aluminum hydroxide.

In general, the comparison of the a_{O2}/a_{C3H8} ratio with the selectivity shows that graphite controlled to some extent the production of active oxygen species that lead to the complete oxidation of propane to CO$_x$. The graphite surface possesses terminal oxygen functional groups that have been found to act as highly alkene selective active sites in ODH.[37,61,67,68] The fact that the influence of graphite on selectivity is more notorious at higher temperature points to a formation of such oxygen functional active groups under the reaction atmosphere. Lower a_{O2}/a_{C3H8} ratios for graphite containing VAlO-*x*G-NC at 748 K support this hypothesis. This phenomenon has been reported for alkane ODH reactions on carbon nanotube based catalysts.[68] On the other hand, as hydroxides, noncalcined

VAlO-*x*G-NCs are prone to liberate significant quantities of molecular water and reactive OH$^-$ radicals during the reaction which can attack the edges of the graphene layers that constitute graphite. The role of water OH$^-$ radicals and hydroxyl surface groups in ODH is far from being fully understood. Reaction kinetic studies conducted by Iglesia and co-workers[69,70] show that water partial pressure during propane ODH influences propene selectivity of supported VO$_x$ catalysts. Particularly, they have postulated that the reversible recombination of water with surface hydroxyls leads to a decrease in the rate of propene formation.[69] The explanation was that water affects oxygen mobility and stabilizes surface reaction intermediates that convert into CO$_x$.[70] Similar phenomena may occur during ODH of propane over VAlO-*x*G-NC with graphite acting as a moderator of the negative impact of water on propene selectivity. More profound studies are likely worthy to better understand the dynamics of ODH reactions over noncalcined VAlO-*x*G-NC.

The behavior of the calcined VAlO-*x*G-C catalysts in ODH differed from that registered for the noncalcined materials. Table 6 shows the steady state catalytic performance of VAlO-*x*G-C at 723 and 748 K. With the exception of VAlO-7G, propane activity for the calcined catalysts was always higher as compared to noncalcined VAlO-*x*G-NC. Graphite was found to improve propane activity compared to pure VAlO-C but following a sort of volcano shape plot with graphite loading, this regardless of reaction temperature. The highest propane activity was obtained over VAlO-3G-C. For pure VAlO, calcination led to a decrease in propene selectivity at 723 K (S_{C3H6} = 0.57, for VAlO-NC; S_{C3H6} = 0.29, for VAlO-C). Selectivity decrease was accompanied by a higher a_{O2}/a_{C3H8} ratio for VAlO-C. At 748 K both catalysts exhibited the same propane activity, but calcined VAlO-C presented higher selectivity (S_{C3H6} = 0.18, for VAlO-NC; S_{C3H6} = 0.24, for VAlO-C) in spite of its higher a_{O2}/a_{C3H8} ratio (a_{O2}/a_{C3H8} = 2.1, for VAlO-NC; a_{O2}/a_{C3H8} = 2.6, for VAlO-C). The selectivity differences between the noncalcined and calcined VAlOs can be explained when considering the above-mentioned effect of water on the catalytic performance. One may recall that the calcined catalysts lost about 33.5 wt % during calcination and that the hydroxides were transformed into a mixed oxide whose structure resembles decavanadate $[V_{10}O_{28}]^{(6-n)}$ and V$_2$O$_5$ within a γ-Al$_2$O$_3$ matrix (Section 3.4. on Raman). On the other hand, it is interesting to notice that in spite that graphite containing calcined VAlO-*x*G-C catalysts was found to be less selective to propene, their propane activity was remarkably higher as compared to VAlO-*x*G-NC, an exception being made for VAlO-7G-NC/C. Such activity difference was strongest for the catalyst containing 3 wt % graphite (up to 1 order of

magnitude at 748 K). This is associated to a higher concentration of surface metallic atoms in the calcined materials as demonstrated by XPS analysis (Table 2). Moreover, XPS also showed that the surface concentration of V−O−Al oxygen species increased after calcination as compared to surface oxygen species bonded to hydroxyls and carbon (Table 4). Besides the structural evolution of the vanadium−aluminum structure of the VAlO-xG materials during calcination, graphite combustion may have also occurred during calcination creating more defects in its graphene layers, thereby increasing the concentration of potential ODH active sites. This assumption agrees with the results presented by Frank et al.[68] for oxidized carbon nanotubes in propane ODH. Also, the role of graphite as a selectivity moderator is more clearly evidenced when one directly compares the individual behavior of each catalyst containing this binding agent. The particular catalytic performance of VAlO-xG-NC/C deserves attention because it serves to support this hypothesis. Regardless of reaction temperature, noncalcined VAlO-7G-NC and calcined VAlO-7G-C displayed the same propane activity (Tables 5 and 6). Though calcined VAlO-7G-C exhibited comparatively larger a_{O2}/a_{C3H8} ratios, it exhibited either the same propene selectivity, at 723 K, or higher selectivity, at 743 K, than noncalcined VAlO-7G-NC. XPS results showed that VAlO-7G-C has a very high concentration of graphite on its surface (Table 3 and Figure 6), which would enhance its control in the dynamics and nature of the generated active oxygen species intervening in the reaction. Moreover, the surface interaction between graphite particles and VAlO significantly changed after calcination.

4. CONCLUSIONS

Aiming to contribute to the construction of a scientific basis for the understanding of the physicochemical and catalytic consequences of shaping catalytic powders, the effect of using graphite as a binding agent for tableting vanadium−aluminum mixed (hydr)oxides was for the first time analyzed. Besides being an effective binding agent, graphite was found to act as a selectivity modifier of vanadium−aluminum mixed (hydr)-oxides. More precisely, graphite was found to favor propylene production in propane ODH. The role performed by graphite in the selectivity in ODH was ascribed to the existence of active sites on its surface and to its intervention in the production of active oxygen species. Graphitic-like amorphous carbon species identified through XPS were associated to the above phenomena. Furthermore, graphite enhanced up to seven times the mechanical resistance of VAlO hydroxides regardless of its loading. The increase in the mechanical resistance was ascribed to the fact that both graphite and VAlO powders are constituted by plate like particles randomly distributed in the shaped catalysts which made them more resistant to compression forces.

Raman analysis of the structure of the amorphous VAlO-xG mixed hydroxides indicated that these materials are constituted by Al(OH)$_3$, AlOOH, polymeric decavanadates and metavana-dates, and isolated or cluster vanadyl V=O species with graphite physically attached to the VAlO particles. Calcination of the VAlO-xG mixed hydroxides led to its transformation into a mixed oxide in which a higher concentration of polymerized vanadium species was present. Such species formed larger decavanate chains and amorphous V$_2$O$_5$-like structures. The aluminum hydroxides were transformed into a γ-Al$_2$O$_3$-like structure thus serving as matrix for the mixed oxide. Within

these structures, most of the vanadium was in the V^{5+} oxidation state. These characteristics contributed to the high activity of the VAlO-xG-NC/C catalysts in propane ODH. Conversely, there was no evidence of an integration of graphite into the lattice of VAlO, but XPS showed that the surface interaction between graphite and VAlO should not be neglected. Finally, burning of graphite to CO$_x$ under the oxidative conditions of ODH and during calcination was discarded on the basis of XPS analysis.

A drawback of tableting was a significant loss in surface area accompanied by pore widening. These changes were accentuated by graphite addition because its presence eased the tableting process through the formation of a lubricant layer between the VAlO particles and the metallic walls of the tableting machine. On the other hand, calcination led to further surface area decrease and cracking of the VAlO-xG tablets. These effects were explained by considering an extensive water loss during the transformation of the mixed VAlO hydroxides into VAlO mixed oxides. A more detailed study on the mechanism of the aforementioned transformations is still required.

■ ASSOCIATED CONTENT

ⓢ Supporting Information

Further details are given in plots of nitrogen adsorption-desorption isotherms and pore size distributions, and on the determination of surface area from N$_2$ physisorption. The methodology employed to verify the absence of mass and heat transfer limitations is provided as well. This material is available free of charge via the Internet at http://pubs.acs.org.

■ AUTHOR INFORMATION

Corresponding Author

*Phone: +32 10473665. Fax: +32 10473649. E-mail: victor.baldovino@uclouvain.be (V.G.B.-M.), eric.gaigneaux@uclouvain.be (E.M.G.).

■ REFERENCES

(1) Gallei, E. F.; Hesse, M.; Schwab, E. In *Handbook of Heterogeneous Catalysis*, 2nd ed; Ertl, G., Knözinger, H., Schüth, F., Weitkamp, J., Eds.; Wiley-VCH: Weinheim, GermanyJ, 2008; Vol.1, p57.

(2) Busca, G. *Chem. Rev.* **2007**, *107*, 5366.

(3) Capes, C. E. In *Handbook of Powder Technology*, 1st ed; Williams, J. C., Allen, T., Eds.; Elsevier Scientific: Amsterdam, The Netherlands, 1980; Vol.1, p40.

(4) Font Freide, J. J. H. M.; Gamlin, T. D.; Graham, C.; Hensman, J. R.; Nay, B.; Sharp, C. *Top. Catal.* **2003**, *26*, 3.

(5) Corma, A.; García, H. *Chem. Rev.* **2003**, *103*, 4307.

(6) Keville, K. M.; Timken, H. K. C.; Ware, R. A.; U.S. Patent No. 5,500,109; Mobil Oil Corp., Fairfax, VA, U.S.A., 1996.

(7) Xu, S.; Mikhailovsky, A. A.; Hollingsworth, J. A.; Klimov, V. I. *Phys. Rev. B* **2002**, *65*, 1.

(8) Lee, S.-C.; Jang, J.-H.; Lee, B.-Y.; Kang, M.-C.; Kang, M.; Choung, S.-J. *Appl. Catal., A* **2003**, *253*, 293.

(9) Ren, D.; Wang, X.; Li, G.; Cheng, X.; Long, H.; Chen, L. *J. Nat. Gas Chem.* **2010**, *19*, 646.

(10) Xue, N.; Olindo, R.; Lercher, J. A. *J. Phys. Chem. C* **2010**, *114*, 15763.

(11) Topka, P.; Karban, J.; Soukup, K.; Jirátová, K.; Solcová, O. *Chem. Eng. J.* **2011**, *168*, 433.

(12) Baldovino-Medrano, V. G.; Le, M. T.; Van Driessche, I.; Bruneel, E.; Gaigneaux, E. M. *Ind. Eng. Chem. Res.* **2011**, *50*, 5467.

(13) Prada Silvy, R.; Blangenois, N.; Hamrouni, M.; Grange, P.; Gaigneaux, E. M. In *Studies in Surface Science and Catalysis.*; Gaigneaux, E. M., Devillers, M., De Vos, D. E., Hermans, S., Jacobs, P. A., Martens, J. A., Ruiz, P., Eds.; Elsevier: Amsterdam, The Netherlands, 2006; Vol. *162*, p 187.

(14) Olea, M.; Florea, M.; Sack, I.; Prada Silvy, R.; Gaigneaux, E. M.; Marin, G. B.; Grange, P. *J. Catal.* **2005**, *232*, 152.

(15) Prada Silvy, R.; Florea, M.; Blangenois, N.; Grange, P. *AIChE J.* **2003**, *49*, 2228.

(16) Martin, A.; Kalevaru, V. N. *ChemCatChem* **2010**, *2*, 1504.

(17) Kung, H. H. In *Advances in Catalysis*; Eley, D. D.; Pines, H.; Haag, W. O., Eds.; Academic Press: New York, 1994; Vol. *40*, p 1.

(18) Cavani, F.; Ballarini, N.; Luciani, S. *Top. Catal.* **2009**, *52*, 935.

(19) Genet, M. J.; Dupont-Gillain, C. C.; Rouxhet, P. G. XPS Analysis of Biosystems and Biomaterials (Personal Communication).

(20) Vannice, M. A.; *Kinetics of Catalytic Reactions*, 1st ed.; Springer: New York, 2005; p 38.

(21) Weisz, P. B.; Prater, C. D. In *Advances in Catalysis*; Frankenburg, W. G., Rideal, E. K., Eds.; Academic Press: New York, 1954; Vol. *6*, p 143.

(22) Brunauer, S.; Emmett, P. H.; Teller, E. *J. Am. Chem. Soc.* **1938**, *60*, 309.

(23) Condon, J. B. *Surface Area and Porosity Determinations by Physisorption Measurements and Theory*, 1st ed.; Elsevier Science: Amsterdam, The Netherlands, 2006; p 59.

(24) Gregg, S. J.; Sing, K. S. W. *Adsorption, Surface Area, and Porosity*, 2nd ed.; Academic Press: New York, 1982; p 94.

(25) Barrett, E. P.; Joyner, L. G.; Halenda, P. P. *J. Am. Chem. Soc.* **1951**, *73*, 373.

(26) Sing, K. S. W. *Pure Appl. Chem.* **1985**, *57*, 603.

(27) de Boer, J. H.; Lippens, B. C. *J. Catal.* **1964**, *3*, 38.

(28) Rouquerol, F.; Rouquerol, J.; Sing, K. *Adsorption by Powders and Porous Solids, Principles, Methodology and Applications*, 1st ed.; Academic Press: San Diego, CA, 1999; p 165.

(29) Morimoto, T.; Miura, K. *Langmuir* **1985**, *1*, 658.

(30) Miura, K.; Morimoto, T. *Langmuir* **1988**, *4*, 1283.

(31) Lee, D. W.; Seo, J. W. *J. Phys. Chem. C* **2011**, *115*, 12483.

(32) Estrade-Szwarckopf, H. *Carbon* **2004**, *42*, 1713.

(33) NIST X-ray Photoelectron Spectroscopy Database, version 3.5. National Institute of Standards and Technology: Gaithersburg, MD, 2003; http://srdata.nist.gov/xps/. (Accessed July–Aug, 2011)

(34) XPS online Database. Benoit, R. D. Y.; Narjoux, B.; Quintana, G.; Georges, Y. CNRS & ThermoFisher Scientific: 2011. http://lasurface.com/. (Accessed July–Aug, 2011).

(35) Weckhuysen, B.; Rosynek, M.; Lunsford, J. *Catal. Lett.* **1998**, *52*, 31.

(36) Blyth, R. I. R.; Buqa, H.; Netzer, F. P.; Ramsey, M. G.; Besenhard, J. O.; Golob, P.; Winter, M. *Appl. Surf. Sci.* **2000**, *167*, 99.

(37) Zhang, J.; Liu, X.; Blume, R.; Zhang, A.; Schlögl, R.; Su, D. S. *Science* **2008**, *322*, 73.

(38) Bismarck, A.; Tahhan, R.; Springer, J.; Schulz, A.; Klapötke, T. M.; Zeil, H.; Michaeli, W. *J. Fluorine Chem.* **1997**, *84*, 127.

(39) Wang, D.; Lunsford, J. H.; Rosynek, M. P. *J. Catal.* **1997**, *169*, 347.

(40) van Attekum, P. M. T. M.; Wertheim, G. K. *Phys. Rev. Lett.* **1979**, *43*, 1896.

(41) Sette, F.; Wertheim, G. K.; Ma, Y.; Meigs, G.; Modesti, S.; Chen, C. T. *Phys. Rev. B* **1990**, *41*, 9766.

(42) Chen, J.-H.; Jang, C.; Xiao, S.; Ishigami, M.; Fuhrer, M. S. *Nat. Nanotechnol.* **2008**, *3*, 206.

(43) Dean, C. R.; Young, A. F.; Meric, I.; Lee, C.; Wang, L.; Sorgenfrei, S.; Watanabe, K.; Taniguchi, T.; Kim, P.; Shepard, K. L.; Hone, J. *Nat. Nanotechnol.* **2010**, *5*, 722.

(44) Hartmanová, M.; Le, M. T.; Van Driessche, I.; Hoste, S.; Kundracik, F. *Russ. J. Electrochem.* **2005**, *41*, 455.

(45) Lee, C.-K.; Cho, E.; Lee, H.-S.; Seol, K. S.; Han, S. *Phys. Rev. B* **2007**, *76*, 245110.

(46) Beke, S.; Kőrösi, L.; Papp, S.; Oszkó, A.; Nánai, L. *Appl. Surf. Sci.* **2009**, *255*, 9779.

(47) Chenakin, S. P.; Prada Silvy, R.; Kruse, N. *J. Phys. Chem. B* **2005**, *109*, 14611.

(48) Silversmit, G.; Poelman, H.; De Gryse, R.; Bras, W.; Nikitenko, S.; Florea, M.; Grange, P.; Delsarte, S. *Catal. Today* **2006**, *118*, 344.

(49) Florea, M.; Prada Silvy, R.; Grange, P. *Appl. Catal., A* **2005**, *286*, 1.

(50) Wiame, H.; Bois, L.; Lharidon, P.; Laurent, Y.; Grange, P. *Solid State Ionics* **1997**, *101−103*, 755.

(51) Colomban, P. *J. Mater. Sci.* **1989**, *24*, 3002.

(52) Ruan, H. D.; Frost, R. L.; Kloprogge, J. T. *J. Raman Spectrosc.* **2001**, *32*, 745.

(53) Tian, H.; Wachs, I. E.; Briand, L. E. *J. Phys. Chem. B* **2005**, *109*, 23491.

(54) Wachs, I. E. In *Metal Oxides: Chemistry and Applications*; Fierro, J. L. G., Ed.; Taylor & Francis: Boca Raton, FL, 2006; p 1.

(55) Magg, N.; Immaraporn, B.; Giorgi, J. B.; Schroeder, T.; Bäumer, M.; Döbler, J.; Wu, Z.; Kondratenko, E.; Cherian, M.; Baerns, M.; Stair, P. C.; Sauer, J.; Freund, H.-J. *J. Catal.* **2004**, *226*, 88.

(56) Martínez-Huerta, M. V.; Gao, X.; Tian, H.; Wachs, I. E.; Fierro, J. L. G.; Bañares, M. A. *Catal. Today* **2006**, *118*, 279.

(57) Temuujin, J. J., Ts.; Mackenzie, K. J. D.; Angerer, Porte, P. F.; Riley, F. *Bull. Mater. Sci.* **2000**, *23*, 301.

(58) Gabelkov, S.; Tarasov, R.; Poltavtsev, N.; Kurilo, Y. *Powder Metall. Met. Ceram.* **2009**, *48*, 478.

(59) Choi, J.; Suh, D. *Catal. Surv. Asia* **2007**, *11*, 123.

(60) Kudin, K. N.; Ozbas, B.; Schniepp, H. C.; Prud'homme, R. K.; Aksay, I. A.; Car, R. *Nano Lett.* **2007**, *8*, 36.

(61) Xie, H.; Wu, Z.; Overbury, S. H.; Liang, C.; Schwartz, V. *J. Catal.* **2009**, *267*, 158.

(62) Klose, F.; Wolff, T.; Lorenz, H.; Seidel-Morgenstern, A.; Suchorski, Y.; Piórkowska, M.; Weiss, H. *J. Catal.* **2007**, *247*, 176.

(63) Schlögl, R. *Top. Catal.* **2011**, 1.

(64) Song, S.; Jiang, S.; Rao, R.; Yang, H.; Zhang, A. *Appl. Catal., A* **2011**, *401*, 215.

(65) Suchorski, Y.; Munder, B.; Becker, S.; Rihko-Struckmann, L.; Sundmacher, K.; Weiss, H. *Appl. Surf. Sci.* **2007**, *253*, 5904.

(66) Heracleous, E.; Lemonidou, A. A. *Catal. Today* **2006**, *112*, 23.

(67) McGregor, J.; Huang, Z.; Parrott, E. P. J; Zeitler, J. A.; Nguyen, K. L.; Rawson, J. M.; Carley, A.; Hansen, T. W.; Tessonnier, J.-P.; Su, D. S.; Teschner, D.; Vass, E. M.; Knop-Gericke, A.; Schlögl, R.; Gladden, L. F. *J. Catal.* **2010**, *269*, 329.

(68) Frank, B.; Morassutto, M.; Schomäcker, R.; Schlögl, R.; Su, D. S. *ChemCatChem* **2010**, *2*, 644.

(69) Chen, K.; Khodakov, A.; Yang, J.; Bell, A. T.; Iglesia, E. *J. Catal.* **1999**, *186*, 325.

(70) Chen, K.; Bell, A. T.; Iglesia, E. *J. Phys. Chem. B* **2000**, *104*, 1292.